J Appl Electrochem (2011) 41:577–587
DOI 10.1007/s10800-011-0266-3

ORIGINAL PAPER

Anodic oxidation of organic pollutants on a Ti/SnO_2–Sb_2O_4 anode

L. Ciríaco · D. Santos · M. J. Pacheco · A. Lopes

Received: 15 November 2010 / Accepted: 16 February 2011 / Published online: 27 February 2011

Abstract A Ti/SnO_2–Sb_2O_4 electrode was prepared by alternate Sn and Sb electrodepositions using the thermo-electrochemical method. The chemical, electrochemical, and structural characterization of the electrode was performed and it was tested in the anodic oxidation of several pollutants, phenol, ibuprofen, acid orange 7 (AO7), and diclofenac, all in aqueous 0.035 M Na_2SO_4 solutions at current densities of 10 and 20 mA cm^{-2}. After the 24 h assay, removal of chemical oxygen demand, total organic carbon (TOC) and absorbance were very high, especially at the higher current density. TOC removals presented the lowest value. However, after 24 h at 20 mA cm^{-2}, TOC removals were: phenol—94%; ibuprofen—83%; AO7—88%; and diclofenac—73%. Combustion efficiency and instantaneous and mineralization current efficiencies were also determined.

Keywords Ti/SnO_2–Sb_2O_4 anode · Anodic oxidation · Phenol · AO7 · Ibuprofen · Diclofenac

1 Introduction

Biological treatment of wastewaters has become the most important process for controlling aquatic environment pollution caused by organic chemicals from municipal and industrial sources. However, because some pollutants are not biodegradable, tertiary oxidation processes can be a solution for the removal of the remaining persistent organic pollutants. Electrochemical processes are among the polishing treatments that can be successfully applied to completely remove the residual organic load from wastewaters. However, it is critical to develop electrodes with a high activity for the oxidation of the pollutants and that have a long life and a low cost.

Pure SnO_2 is an n-type semiconductor, with a band gap of about 3.5 eV, which cannot be used directly as electrode material due to its high resistivity at room temperature. Nevertheless, when doped with Ar, B, Bi, F, P, or Sb, its conductivity increases considerably [1–6]. There have also been attempts to use less common elements as doping agents, like Ir, Rh, and various lanthanides [7–12].

Antimony is the most commonly used dopant in SnO_2 electrodes. The behavior of SnO_2 and Sb-doped SnO_2 as anodes has been previously investigated and compared with that of several electrode materials like boron-doped diamond (BDD) [1, 13–24].

Comninellis [25] has investigated different anode materials, namely Pt, Ti/IrO_2, and Ti/SnO_2, in the electrochemical conversion/combustion of several organic pollutants. Simplified mechanisms for electrochemical oxidation and combustion were presented, being the first step of the mechanism the discharge of water molecules to form $^{\bullet}OH$ radicals:

$$MO_x + H_2O \rightarrow MO_x(^{\bullet}OH) + H^+ + e^- . \quad (1)$$

Depending on the nature of the electrode material (MO_x), selective oxidation (for "active" electrodes) or combustion (for "non-active" electrode) can occur. The Ti/SnO_2 has been considered "non-active" electrode since Sn(IV) is the highest oxidation state. This anode has high overvoltage for oxygen evolution reaction and can promote the oxidation of organic compounds by highly reactive OH radicals, generated at the electrode surface [25].

L. Ciríaco (✉) · D. Santos · M. J. Pacheco · A. Lopes
UMTP and Department of Chemistry, University of Beira Interior, 6201-001 Covilhã, Portugal
e-mail: lciriaco@ubi.pt

The performance of doped SnO_2 electrodes is believed to be superior to Pt, graphite, PbO_2, and many other common electrodes, due to its higher current efficiency and because the oxidation reactions on the SnO_2 electrode are very unselective, which gave this electrode the possibility of being applied to a multitude of different wastewaters [1, 13, 15, 26].

The anodic oxidation of phenol was performed on different electrode materials and a SnO_2–Sb_2O_5 electrode showed the highest ability to completely oxidize phenol among PbO_2, IrO_2, RuO_2, and Pt, and with a current efficiency over three times higher than for the other electrodes [16]. In addition, the behavior of a Ti/SnO_2–Sb_2O_5 electrode in the electrodegradation of phenol in the presence of NaCl was studied and compared with that of a Ti/IrO_2 electrode, but the catalytic effect attributed to ClO^- was only verified with the Ti/IrO_2 electrode [27].

Ti/SnO_2 and Ti/IrO_2 anodes were also used in the oxidation of 1,4-benzoquinone [28]. With Ti/IrO_2, non-toxic carboxylic acids were obtained as final products, while these carboxylic acids were oxidized to CO_2 with Ti/SnO_2.

Polcaro et al. [29] compared the performance of Sb-doped Ti/SnO_2 and Ti/PbO_2 anodes in the electrochemical degradation of 2-chlorophenol and concluded that Ti/SnO_2 presented a better ability to oxidize toxic compounds. These two electrode materials were also used in the electrochemical treatment of landfill leachate, but did not show substantial differences under the experimental conditions used [14]. A Ti–SnO_2–Sb_2O_5 electrode, prepared by the thermal method, and a BDD electrode were used in the anodic oxidation of acetic acid, maleic acid, and phenol [30]. Interestingly, the BDD electrode presented a higher current efficiency and service-life. Furthermore, a mixed oxide electrode of Ti/SnO_2–Sb_2O_3–Nb_2O_5/PbO_2 was applied to the oxidation of phenol with good performance [31]. The SnO_2–Sb_2O_3 layer was obtained by dipping and annealing at 450 °C under an influx of oxygen, followed by Nb_2O_5/PbO_2 electrodeposition. Recently, the anodic oxidation of 4-chloro-3-methylphenol in aqueous solution using Ti/SnO_2–Sb/PbO_2 electrodes was investigated [32]. PbO_2 was used because it is a cheap material, easy to prepare and has low resistivity, good chemical stability and, with a $SnO_2 + Sb_2O_3$ interlayer, increased lifetime and electrocatalytic activity.

Many of the variations in the preparation of SnO_2 electrodes are meant to extend the lifetime, a problem associated with the performance of the Ti/SnO_2 electrodes. In fact, even when coated with films, the Ti substrate can be oxidized either during the preparation process or when working as an anode, due to film porosity that makes the electrode permeable to oxygen. Therefore, to avoid TiO_2 interlayer formation, which presents high resistivity, many studies have been performed and several proposals have been presented, including the addition of Pt to the SnO_2 film [33–36], a prior platinization of the Ti substrate followed by SnO_2 deposition [37], an addition of IrO_2 or a isomorphous structure interlayer [7, 38–41] or a RuO_x [41] or Sb_2O_x interlayer [42, 43] between the Ti and SnO_2. All of these procedures increased the lifetime of the electrodes, in some cases up to two orders of magnitude longer [38].

Recently, Ti/SnO_2 anodes were prepared by chemical vapor deposition (CVD) without O_2 as a precursor, avoiding the formation of the TiO_2 passivation layer [44]. These electrodes presented a compact microstructure with high overpotential for oxygen evolution and a superior activity for pollutant oxidation. Although a higher surface area should lead to improved catalytic properties in this electrode (as in BDD) prepared by CVD, the surface area was smaller than when prepared by conventional methods, but the catalytic properties were still improved. In another recent report in this area, Sb-doped SnO_2 electrodes were prepared by two different methods, electrodeposition followed by thermal oxidation, which gave a nanocoated material, and by a dip-coating method, where a non-coated material was obtained [45]. When comparing the performance of both these electrodes, the nanocoated electrode gave a faster and higher phenol and TOC removals, probably due to the larger specific surface area and oxygen adsorption.

The various studies found in the literature have shown that doped Ti/SnO_2 is a very promising material for the electrodegradation of organics, due to its unselective character toward anodic oxidation and also because of its low price, especially when compared to BDD. However, its main disadvantage is the low stability under anodic polarization. Therefore, the objective of this study was to study the stability of Ti/SnO_2–Sb_2O_4 electrodes, prepared by the thermo-electrochemical method, which involves alternate Sn and Sb electrodepositions. This study also aims to test these electrodes as anodes in the electrochemical degradation of different classes of persistent organic pollutants and evaluate the obtained combustion efficiencies. The chosen organic compounds were phenol, frequently used as a model compound, ibuprofen, a pharmaceutical drug, AO7, an azo dye, and diclofenac, another pharmaceutical drug and the only compound in this group that contains chlorine in its structure.

2 Materials and methods

2.1 Chemicals

The following reagents were used, as purchased, in the preparation of the electrodes: titanium foil, 0.25 mm thick, 99.7%, Sigma-Aldrich; sodium hydroxide, 96.8%, Pronalab; oxalic acid, 99%, Merck; chloridric acid, 37%,

Pronalab; tin (II) chloride, 98%, Sigma-Aldrich; antimony (III) chloride, 99%, Fluka; and citric acid 100%, Pronalab. The chemicals used as model pollutants and electrolytes were AO7, 85%, Aldrich; sodium ibuprofen salt (IBU), 99.8%, Sigma-Aldrich; sodium diclofenac salt (DIC), 99%, Sigma-Aldrich; phenol (Ph), 99.5%, Merck; and sodium sulfate, 99%, Merck.

2.2 Preparation of Ti/SnO_2–Sb_2O_4 anodes

Ti substrates, with dimensions of 2 cm × 2.5 cm × 0.25 mm, were pre-treated with a mechanical polishing followed by etching with 40% NaOH (w/w) at 80 °C for 2 h and with 15% oxalic acid (w/w) at 98 °C for 1 h. The substrates were then washed with doubly distilled water.

The alternate Sn and Sb electrodeposition on the Ti substrate was carried out in a double wall cell of one compartment connected to a thermostatic water-bath, with recirculation, containing a Ti substrate used as the cathode between two Pt anodes. A 100 mL volume of an aqueous solution with 0.948 g of $SnCl_2$ and 2 mL of concentrated chloridric acid was used with a current density of 10 mA cm^{-2} maintained for 2 h 45 min at 35 °C for the Sn deposition. For the Sb deposition, a volume of 100 mL of an aqueous solution with 1.329 g of $SbCl_3$ and 3.842 g of citric acid was used and a current density of 10 mA cm^{-2} was applied for 30 min at 35 °C. These two procedures were repeated four times. After this treatment, the electrodes were heated in a tubular furnace at 550 °C for 3 h to obtain the respective oxides. The geometric area of the prepared electrodes was 10 cm^2 (both sides).

2.3 Characterization of the electrodes

Electrodes were structurally characterized by X-ray powder diffraction (XRD) at room temperature using a Rigaku DMAXIII/C diffractometer with Cu K_α radiation (λ = 0.15406 nm) and working at 30 kV/40 mA. The diffraction patterns were collected in the range of 2θ = 10–90° with a 0.02° step and an acquisition time of 2 s/step. Their morphology was then characterized by scanning electron microscopy (SEM), and the microanalysis was performed by dispersive energy spectroscopy (EDS) in a Hitachi (S-2700)/Oxford (60–74) system operating at 20 keV.

The cyclic voltammetric measurements were performed in a potentiostat/galvanostat VoltaLab PGZ 301 in an one compartment cell with a 10 cm^2 Ti/SnO_2–Sb_2O_4 electrode as the working electrode, a 5 cm^2 (each side) platinum plate as the counter electrode and a commercial saturated Ag/AgCl, KCl_{sat} electrode as the reference electrode. Voltammograms were recorded at 20 and 50 mV s^{-1} in 0.035 M Na_2SO_4 aqueous solution with pollutant concentrations varying between 0.2 and 1.5 g L^{-1}.

2.4 Electrodegradation assays

Electrodegradation experiments were conducted in a 250 mL undivided cell using batch mode with stirring. The anode was a Ti/SnO_2–Sb_2O_4 electrode and the cathode a stainless steel foil, both electrodes being 10 cm^2 in area and having a 1 cm gap between them. All anodic oxidation assays were performed under galvanostatic conditions with imposed current densities of 10 and 20 mA cm^{-2}. The processed solution volume was 200 mL with a concentration of 100 mg L^{-1} for IBU, AO7, and DIC, and 200 mg L^{-1} for phenol. Sodium sulfate aqueous solutions (0.035 M) were used as the supporting electrolyte in all experiments. Assays were run for 24 h, and data points were collected at 2 h intervals during the first 8 h with a final one collected at 24 h. The degradation of the organic pollutants was followed by UV–Visible absorption spectrophotometry with absorbance measurements between 200 and 800 nm using a *UNICAM Helios-α UV/VIS* spectrophotometer. Chemical oxygen demand (COD) determinations were made using the titrimetric method with closed reflux [46]. The decrease in organic carbon content during the assays was monitored by measurements of the total organic carbon (TOC), performed in a Shimadzu TOC-$V_{CPH/CPN}$ apparatus. All of the assays were repeated twice, and COD and TOC values presented are presented as mean values.

3 Results and discussion

3.1 Electrode characterization

3.1.1 Structural characterization by XRD

After calcination at 550 °C, a X-Ray diffractogram was obtained (Fig. 1a) and compared with those from the JCPDS ICDS database. The presence of two phases, Sb_2O_4 (file PDF#11-0694, relative to an orthorhombic structure with a = 5.436 Å, b = 4.81 Å, and c = 11.76 Å) and SnO_2 (file PDF# 41-1445, tetragonal structure with $a = b$ = 4.7382 Å and c = 3.1871 Å) were confirmed. It could therefore be concluded that, with the experimental conditions used, the obtained oxides were tin (IV) oxide, and antimony tetroxide in the oxidation states of (III) and (V), similar to the electrodes prepared for another study [42].

3.1.2 Morphological characterization by SEM

Figure 1c contains the micrographs of the Ti/SnO_2–Sb_2O_4 electrode after the final calcination at different magnifications. The material presented characteristic aspects of

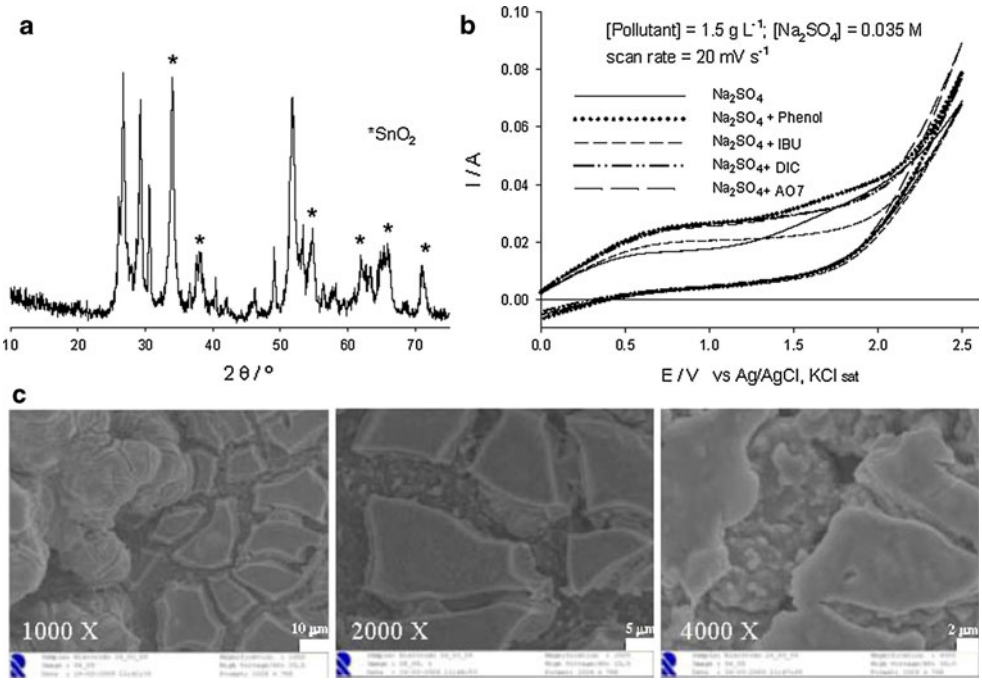

Fig. 1 **a** X-ray diffractogram of the $Ti/SnO_2–Sb_2O_4$ electrode in its final form after calcination at 550 °C, **b** cyclic voltammogram for the system $Ti/SnO_2–Sb_2O_4/Na_2SO_4$ (0.035 M) or Na_2SO_4 (0.035 M) + pollutant (1.5 g L^{-1}). Scan rate of 20 mV s^{-1}, **c** micrographs of the $Ti/SnO_2–Sb_2O_4$ electrode after the final calcination at 550 °C with different magnification (×1000, ×2000, and ×4000)

cracked mud, having already been referred to by other authors [37, 41].

3.1.3 Chemical characterization by EDS

The results from the EDS analysis of the final stage of the electrodes preparation, in atomic molar percentages, were the following: O—71%, Sn—11%, and Sb—18%. These results corresponded to a composition for the material of 36.5% SnO_2 and 63.5% Sb_2O_4. The Sb_2O_4 content, which was higher than expected, may be due to the fact that the final layer consisted of antimony, which is more easily detected by EDS.

3.1.4 Electrochemical characterization by cyclic voltammetry

To avoid the reduction of Sn or Sb at the electrode surface, voltammetries were only run for potentials higher than −0.5 V. Although voltammograms for the system $Ti/SnO_2–Sb_2O_4/Na_2SO_4$ (0.035 M) were run for different organics concentrations and scan rates, the best defined peaks were obtained for the concentration 1.5 g L^{-1} at a scan rate of 20 mV s^{-1} (Fig. 1b). In addition to an increase in anodic current up to $E = 0.6$ V versus Ag/AgCl, KCl_{sat}, probably due to the oxidation of Sb(III) to Sb(V), a shoulder due to the oxidation of sulfate to persulfate appeared. This feature arose at 1.724 V versus Ag/AgCl, KCl_{sat} at pH 7 [47]. Very high overpotentials for oxygen evolution were also noted at 1.8 V versus Ag/AgCl, KCl_{sat}, in agreement with what was observed by Cui et al. [24], suggesting that this material has the potential for anodic oxidation of organic pollutants.

Figure 1b presents the cyclic voltammetries performed with the $Ti/SnO_2–Sb_2O_4/Na_2SO_4$ (0.035 M) + pollutant (1500 mg L^{-1}) system at a scan rate of 20 mV s^{-1}. As can be observed, in the presence of the pollutant there is an increase in current in all of the anodic ranges, even in the oxygen evolution region, except for ibuprofen. This increase may be due to the oxidation of the pollutant molecule. According to these results, all pollutants except ibuprofen could compete with water oxidation at current densities higher than approximately 4 mA cm^{-2}. However, to perform the complete oxidation of the studied pollutants, as well as the metabolites that may result from the first steps of the oxidation, and to avoid the electrode surface passivation that happens for low applied potentials, the electrodegradation assays were run at the higher current densities of 10 and 20 mA cm^{-2}, thus guaranteeing an applied potential high enough to allow the complete oxidation of organics and to prevent passivation.

The relative roughness factor [48], R_f, of the electrode coating was estimated by running cyclic voltammetric curves with the $Ti/SnO_2–Sb_2O_4$ electrode as the working electrode in an one compartment electrochemical cell. Since the electrode was made of conductive oxides, there must be a linear dependence between the double layer charging currents, I, and the scanning rates, υ, closely related to the double layer capacitance, C, of the electrode/solution interface. Figure 2 presents several cyclic voltammograms recorded at different scan rates between 2 and 10 mV s^{-1} in 0.035 M Na_2SO_4 aqueous solutions between

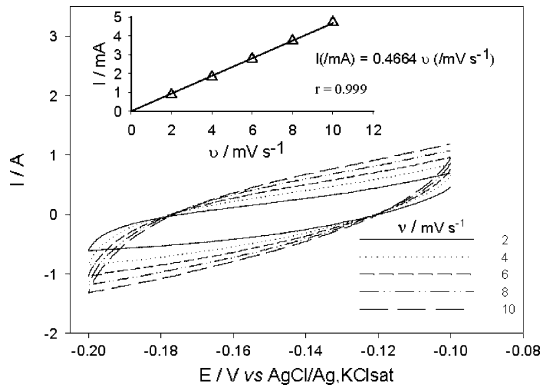

Fig. 2 Cyclic voltammogram obtained at the double layer region for different scan rates between 2 and 10 mV s^{-1} with a 0.035 M Na_2SO_4 solution (*inset* linear regression of I vs. υ measured at $E = -0.15$ V)

-0.2 and -0.1 V versus Ag/AgCl, KCl_{sat}. As can be seen, only double layer charging currents were subsequently observed. From the above-mentioned current–potential curves, I values for different scan rates were obtained at $E = -0.15$ V versus Ag/AgCl, KCl_{sat}, a point where an approximate symmetry of anodic and cathodic currents was observed. From the plot of I versus υ (see inset in Fig. 2) the following linear equation was obtained:

$$I(\text{mA}) = 0.4664\upsilon(\text{mV s}^{-1}), \quad \text{with } r^2 = 0.999. \qquad (2)$$

Dividing the slope value, 0.4664 F, by the geometric area of the electrode, the normalized capacitance of the oxide/solution interface ($C = dq/dE = dI/d\upsilon$), $C_{Ti/SnO_2-Sb_2O_4} = 0.0466$ F cm^{-2}, can thus be obtained. To estimate the relative roughness factor of the Ti/SnO_2–Sb_2O_4 film, its capacitance was compared with that of an oxide with a smooth surface, which was assumed to be 60 μF cm^{-2} [48], providing a $R_f = 777$ for the prepared material. This value was roughly on the same order of magnitude of other roughness factors presented in the literature for oxides [49].

3.2 Electrodegradation assays

3.2.1 *Phenol*

Figure 3 presents the experimental result obtained in the degradation of phenol. The absorption spectra for the assays run at the different current densities, depicted in Fig. 3a, b, showed a regular decay in absorbance at the characteristic wavelengths, particularly 210 nm. However, there was a broadening of the band at 268 nm, probably due to the formation of polymeric substances frequently observed during the anodic oxidation of phenol [50]. For the experiment run at 10 mA cm^{-2}, even after 24 h the removal of absorbance at both wavelengths was lower than 60%. This fact must be related to the passivation of the electrode by polymers formed at its surface, an effect that was partially avoided when higher current density, and,

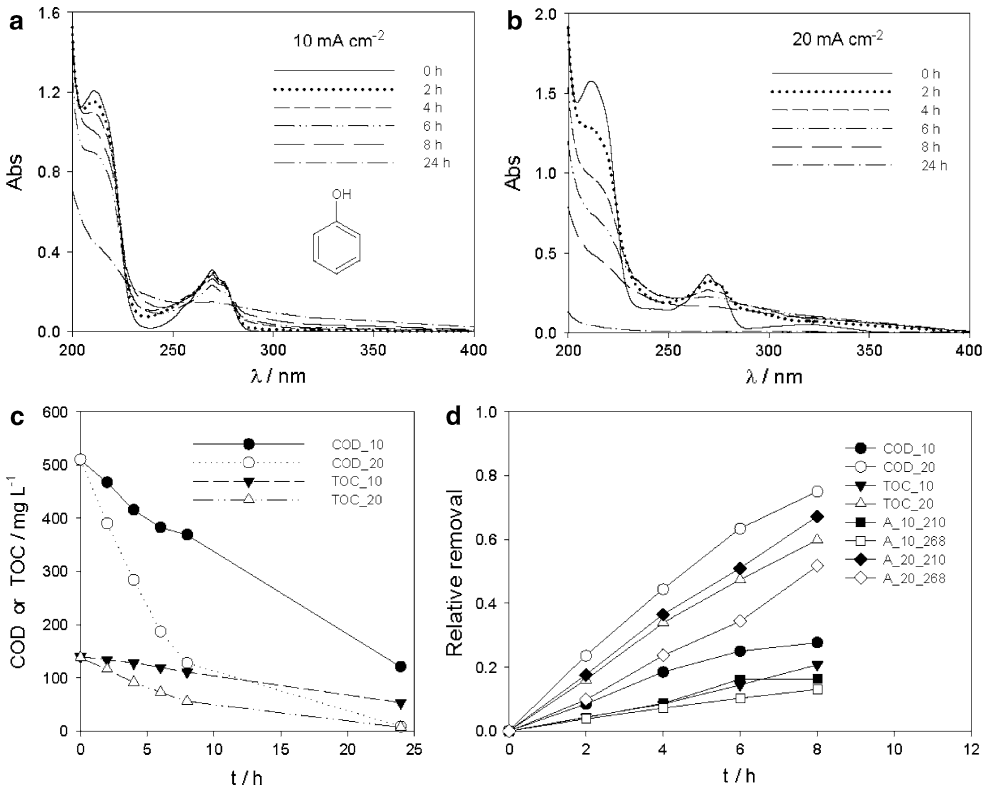

Fig. 3 **a**, **b** UV–Vis absorption spectra, **c** COD and TOC decay, and **d** relative removal of COD, TOC and absorbance (A) measured at 210 and 268 nm for the electrodegradation assays of phenol (200 mg L^{-1} in 200 mL of 0.035 M Na_2SO_4 aqueous solution) run at two different current densities, 10 and 20 mA cm^{-2}. Anode—Ti/SnO_2–Sb_2O_4 (10 cm^2); cathode—stainless steel foil (10 cm^2)

Table 1 Kinetic constants, experimental slopes of the linear fit of TOC versus COD and combustion efficiencies (η_C) calculated using Eq. 4 for the degradation of the different organic compounds at 10 and 20 mA cm^{-2}

Compounds	Current density (mA cm^{-2})	k_{app} (10^{-5} s^{-1})	Slope TOC versus COD	η_C
Phenol	10	1.2 (0.98)	0.124	0.39
	20	4.7 (0.99)	0.214	0.67
Ibuprofen	10	0.8 (0.98)	0.133	0.45
	20	3.5 (0.99)	0.096	0.32
AO7	10	2.3 (0.99)	0.136	0.39
	20	3.7 (0.99)	0.136	0.39
Diclofenac	10	–	0.267	0.79
	20	–	0.145	0.43

The values in brackets are for correlation coefficients (R^2)

consequently, higher applied potential, was used (the absorbance removal was almost complete after 24 h at 20 mA cm^{-2}).

In Fig. 3c, the decay of COD and TOC versus time is depicted. The increase in current density played an obvious role in the oxidation rate, as the removal of both parameters after 24 h was almost complete. For the first 8 h assay, an exponential equation could be fit to the experimental COD versus time data:

$$\ln \mathrm{COD} = \ln \mathrm{COD}_0 - k_{app}\, t. \quad (3)$$

This equation showed pseudo first order kinetics with an apparent kinetic constant k_{app}, in s^{-1}, that depended on the current intensity (Table 1). In Eq. 3, COD_0 stands for initial COD and t is the time, in seconds. Furthermore, even after 8 h, the removal of COD and TOC (Fig. 3d) were very high, particularly for 20 mA cm^{-2}. The difference in COD and TOC removals in the same assay points to a degradation where the combustion of the pollutant is not complete, especially at 10 mA cm^{-2}. In this figure, it is also worth noting the unusual fact that the decrease in absorbance was lower than the removal of the organic load.

3.2.2 Ibuprofen

In Fig. 4a and b, the absorption spectra for the samples collected during the electrodegradation of IBU are presented, showing a regular decay with time that was more obvious at higher current density. This increase in the absorbance removal with current density was also observed for COD and TOC removal rates (Fig. 4c). Equation 3 was also fit to COD versus time data, and the k_{app} values thus obtained are presented in Table 1. The COD removal also followed pseudo first order kinetics, with the influence of current intensity being even more evident in this case than in phenol degradation. In fact, except for the absorbance measurements at 260 nm, there was a very marked influence of current density on the removal rate of the studied parameters (Fig. 4d). In the case of absorbance at 260 nm, an increase in absorbance was observed with time for both current densities. This phenomenon was probably due to the formation of intermediates that also absorbed at the measured wavelength. In addition, the band with a maximum at 260 nm displayed a broadening, in particular for the lower current density. This observation is usually caused by the formation of polymeric structures, whose formation is enhanced by low current densities.

3.2.3 AO7

The experimental results obtained in the electrodegradation assays performed with the dye AO7 are presented in Fig. 5. The absorption spectra show an almost complete absorbance removal after 8 h, especially for the assay performed at 20 mA cm^{-2} (Fig. 5a, b). COD and TOC removals also increased with current density (Fig. 5c). However, the current intensity influence was less apparent, as can be gathered from the values of k_{app} listed in Table 1, which resulted from the adjustment of Eq. 3 to experimental COD versus time data. The kinetics were pseudo first order in this case as well.

When relative removals of all the studied parameters were compared (Fig. 5d) independently of the applied current density, several conclusions could be drawn. First, the combustion efficiency must be low because the COD removal rate was always higher than the TOC removal rate. This conclusion was corroborated by the fact that, at both wavelengths, absorbance removal rates were higher than that of COD, meaning that bonds responsible for absorbance at the chosen wavelengths were being broken. This breakage then gave origin to other smaller organic compounds in addition to carbon dioxide. Second, the removal rate of the absorbance measured at 486 nm was higher than that measured at 230 nm, meaning that the azo bond, absorbing at 486 nm, was more easily broken than the aromatic bonds, which absorb at 230 nm.

3.2.4 Diclofenac

The results obtained in the anodic oxidation of diclofenac are depicted in Fig. 6. Regarding the absorption spectra (Fig. 6a, b), there was a regular decay of absorbance with

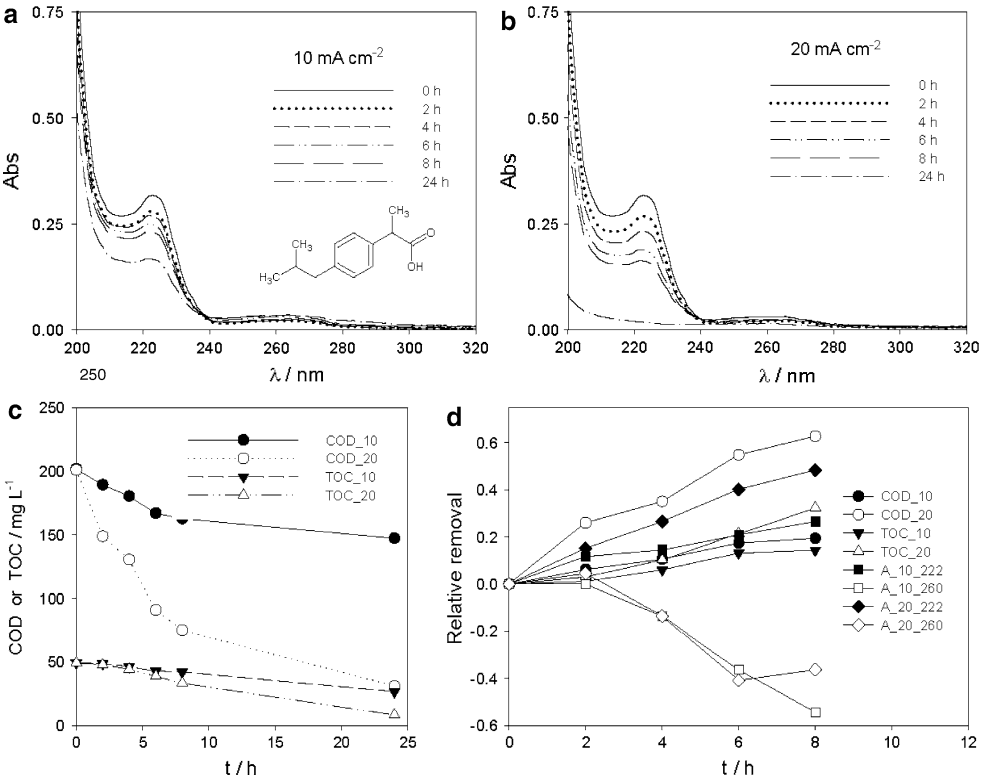

Fig. 4 **a**, **b** UV–Vis absorption spectra, **c** COD and TOC decay, and **d** relative removal of COD, TOC and absorbance (*A*) measured at 222 and 260 nm for the electrodegradation assays of ibuprofen (100 mg L^{-1} in 200 mL of 0.035 M Na_2SO_4 aqueous solution) run at two different current densities, 10 and 20 mA cm^{-2}. Anode—Ti/SnO_2–Sb_2O_4 (10 cm^2); cathode—stainless steel foil (10 cm^2)

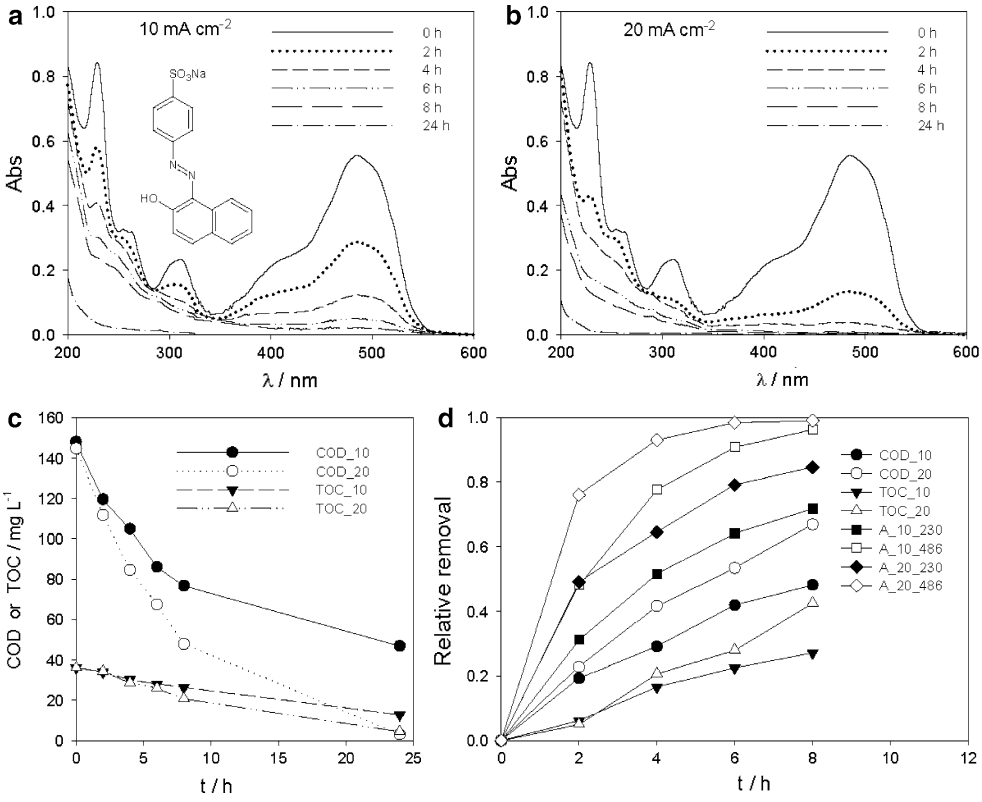

Fig. 5 **a**, **b** UV–Vis absorption spectra, **c** COD and TOC decay, and **d** relative removal of COD, TOC and absorbance (*A*) measured at 230 and 486 nm for the electrodegradation assays of AO7 (100 mg L^{-1} in 200 mL of 0.035 M Na_2SO_4 aqueous solution) run at two different current densities, 10 and 20 mA cm^{-2}. Anode—Ti/SnO_2–Sb_2O_4 (10 cm^2); cathode—stainless steel foil (10 cm^2)

time, which was more pronounced for the highest applied current density, especially during the first part of the assay. This behavior was similar to what was observed for the degradation of the other pollutants tested. However, for the COD and TOC results (Fig. 6c), there was a significant difference between the results obtained for this compound

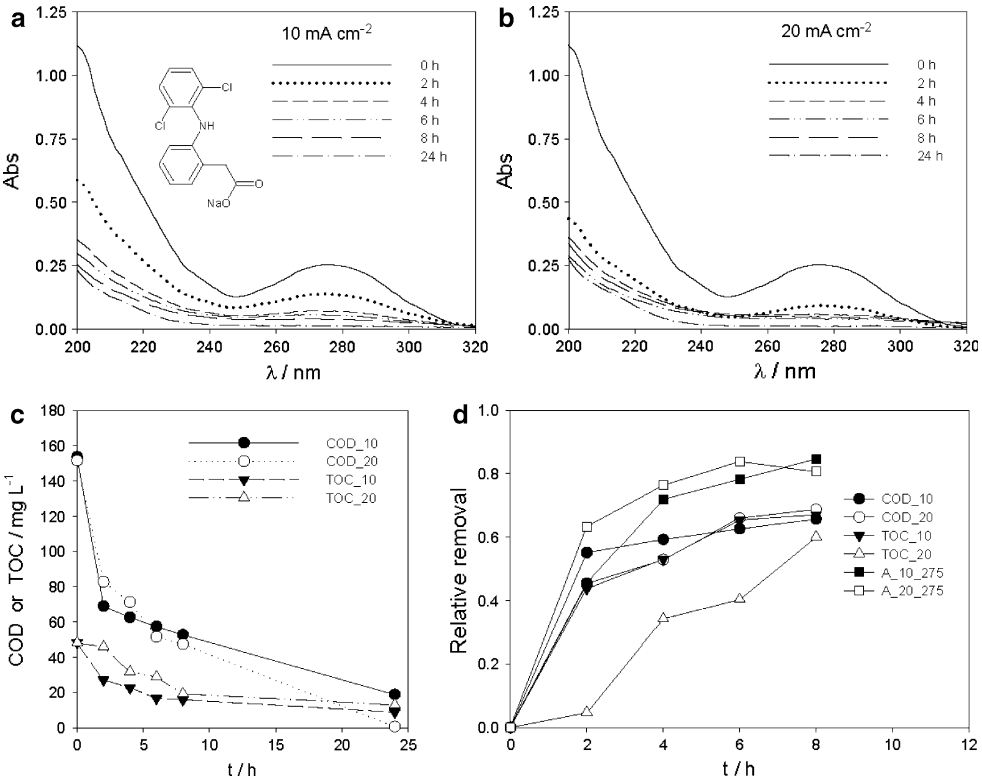

Fig. 6 **a**, **b** UV–Vis absorption spectra, **c** COD and TOC decay, and **d** relative removal of COD, TOC and absorbance (*A*) measured at 275 nm for the electrodegradation assays of diclofenac (100 mg L^{-1} in 200 mL of 0.035 M Na_2SO_4 aqueous solution) run at two different current densities, 10 and 20 mA cm^{-2}. Anode—Ti/SnO_2–Sb_2O_4 (10 cm^2); cathode—stainless steel foil (10 cm^2)

and for the others. In fact, in the first 8 h, the COD removal rate was almost independent of current density and the TOC removal rate only slightly decreased with current density. Another special feature presented by this assay was the abrupt decrease in COD during the first 2 h of the experiment that prevented fitting of Eq. 3 to the experimental data. This behavior is often observed during the anodic oxidation of pollutants containing chlorine in its structure or when chloride salts are used as the electrolyte, as hypochlorite is formed at lower electrochemical potentials than other possible oxidants, like persulfate or hydroxyl radicals [51]. Furthermore, the absorbance removal at 275 nm was much low at the lowest current density, but very similar to the removals of COD and TOC for the same applied current density (Fig. 6d). These observations implied that the diclofenac combustion efficiency must be high at these experimental conditions. On the other hand, the mineralization for the applied current density of 20 mA cm^{-2} was much smaller than at 10 mA cm^{-2}, since the difference between COD and TOC removals increase with the applied current density.

3.3 Determination of combustion and current efficiencies

The degree of combustion could be estimated by determining the ratio between TOC and COD decay, dTOC/dCOD [52]. According to this method, combustion efficiency, η_C, is given by:

$$\eta_C = \frac{32}{12}\left(\frac{n}{4x}\right)\frac{\mathrm{dTOC}}{\mathrm{dCOD}}, \quad (4)$$

where TOC is in $mg_C\ L^{-1}$, COD in $mg_{O_2}\ L^{-1}$, n is the number of electrons transferred to the electrode in the process of the complete combustion of the organic pollutant molecule, and x is the number of carbon atoms of the organic compound. The electrochemical combustion reactions of the studied compounds are then:

$$\text{Phenol: } C_6H_6O + 11H_2O \rightarrow 6CO_2 + 28H^+ + 28e^- \quad (5)$$

$$\text{Ibuprofen: } C_{13}H_{17}O_2Na + 24H_2O \rightarrow 13CO_2 + Na^+ + 65H^+ + 66e^- \quad (6)$$

$$\text{AO7: } C_{16}H_{11}N_2SO_4Na + 32H_2O \rightarrow 16CO_2 + 2NH_4^+ + SO_4^{2-} + Na^+ + 67H^+ + 68e^- \quad (7)$$

$$\text{Diclofenac (assuming that Cl is oxidized to } OCl^-\text{): } C_{14}H_{10}NCl_2O_2Na + 28H_2O \rightarrow 14CO_2 + NH_4^+ + 2OCl^- + Na^+ + 62H^+ + 62e^-. \quad (8)$$

To establish the experimental dTOC/dCOD values, linear fits were used for the TOC versus COD experimental data and the slopes were determined (Fig. 7). In this calculation, only experimental data for the two first hours were used to minimize the influence of the intermediates that formed

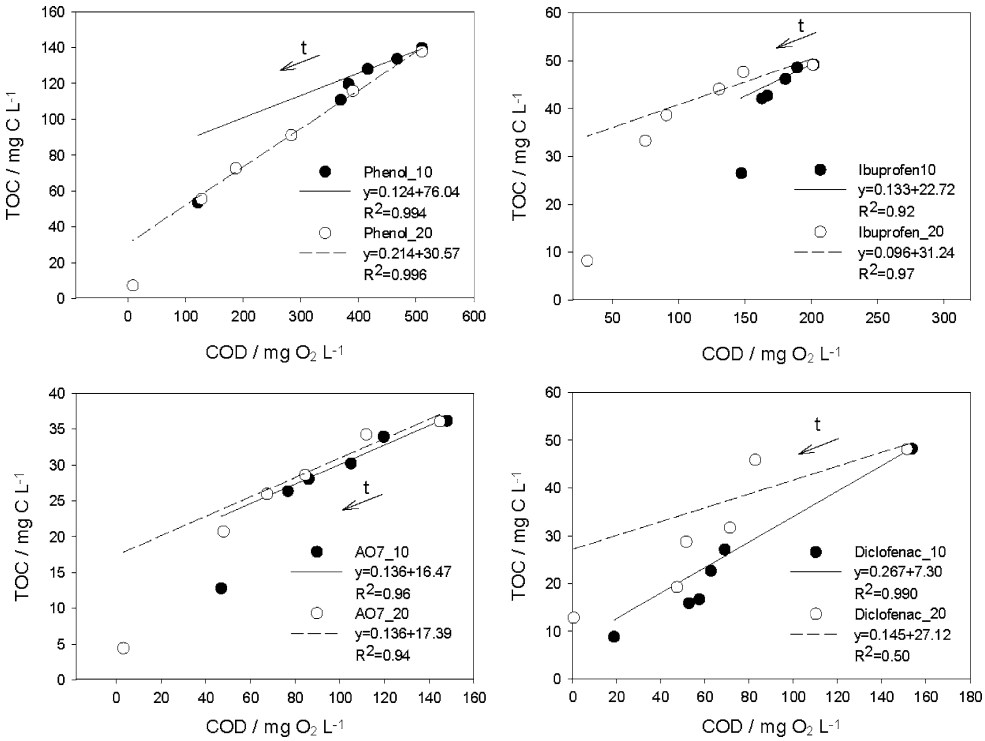

Fig. 7 TOC versus COD evolution in experiments of anodic oxidations of the studied organic compounds, as well as linear fits, at the two applied current densities (10 and 20 mA cm^{-2})

during the anodic oxidation. The values for the combustion efficiency of the different studied compounds, calculated with the slopes from Fig. 7 and using Eq. 4, are presented in Table 1, as well as all of the data needed to calculate η_C. In general, the combustion efficiency was low in all of the studied cases and was independent of the applied current density only for AO7.

Combustion efficiency was already calculated for the anodic oxidation of phenol [52] at a BDD electrode at 10 and 30 mA cm^{-2}. The obtained η_C values were, respectively, 0.41 and 0.87, which were in agreement with those obtained in this study. For ibuprofen, there are also values in the literature [49] calculated for BDD and Ti/Pt/PbO_2 electrodes at 20 mA cm^{-2} (0.99 and 0.87, respectively). These authors also calculated the combustion efficiency with the same electrodes at 30 mA cm^{-2} and obtained $\eta_C = 1$ for both electrode materials. These results were completely different from those obtained in this study because η_C was less than half of the value presented in that study for Ti/SnO_2–Sb_2O_4 anodes [49] and decreased with applied current density, contrary to what was reported for the other electrode materials. In fact, at 10 mA cm^{-2}, the overlap between the removals of absorbance, COD and TOC can be observed for IBU (Fig. 4d). However, because the absolute removals of these parameter were very low, the small absolute differences corresponded to high relative differences and to low combustion efficiency.

The low combustion efficiency obtained for AO7 was expected because the azo bond is oxidized more easily, leading to COD decay without any reduction in TOC. This fact can be observed in Fig. 5d, where the removals for both current densities of the studied parameters were as follows: absorbance (486 nm) > absorbance (230 nm) > COD > TOC.

In the case of diclofenac, the highest value observed for η_C was at 10 mA cm^{-2}, which then decreased sharply with increases in current density. This behavior was due to the low TOC removal at 20 mA cm^{-2} when compared with COD removal and could be explained by the favored formation of oxidized intermediates more resistant to mineralization at higher currents.

In parallel to the above studies, the instantaneous current efficiency [53] (ICE) and the mineralization current efficiency [54] (MCE) could also be calculated using the following equations:

$$\mathrm{ICE} = \mathrm{FV}\left(\frac{\mathrm{COD}_t - \mathrm{COD}_{t+\Delta t}}{8I\Delta t}\right) \quad (9)$$

$$\mathrm{MCE} = \frac{\Delta \mathrm{TOC}_{\mathrm{exp}}}{\Delta \mathrm{TOC}_{\mathrm{theor}}}. \quad (10)$$

where F is the Faraday constant, V is the volume of the solution in m^3, I is the current intensity, t is the time in seconds, $\Delta \mathrm{TOC}_{\mathrm{exp}}$ is the experimental TOC removal and $\Delta \mathrm{TOC}_{\mathrm{theor}}$ is the theoretical TOC decay assuming that the applied electrical charge is only consumed in the mineralization process of the pollutant. The results for ICE and MCE are plotted in Fig. 8 for both applied current

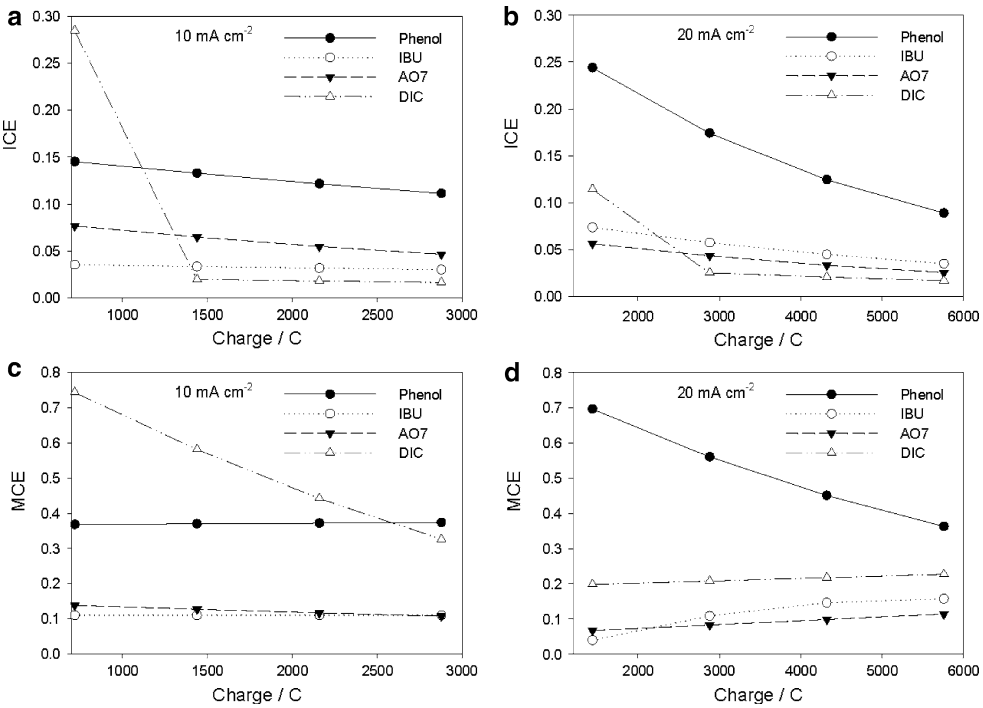

Fig. 8 **a**, **b** ICE and **c**, **d** MCE as a function of the charge passed during electrolysis for the different pollutants studied. phenol (200 mg L^{-1} initial concentration) and IBU, AO7, and DIC (100 mg L^{-1} initial concentration) performed with Ti/SnO_2–Sb_2O_4 anode (10 cm^2) at two different current densities (10 and 20 mA cm^{-2}). Cathode—stainless steel foil (10 cm^2); electrolyte—0.035 M Na_2SO_4 aqueous solution

densities. ICE, for all of the tested pollutants and for both current densities used, was always lower than 30%, which pointed to electrodegradations that were not fully controlled by the current. However, the influence of current density on phenol, IBU, and AO7 was evident from the k_{app} values. In the case of DIC, ICE decreased with current density, pointing to a process where the diffusion played a more important role, which agreed with the observation that the COD removal rate was almost independent of current density. Moreover, although MCE and η_C have different meanings, the conclusions obtained from both parameters were similar (i.e., the highest value at 10 mA cm^{-2} was observed for DIC, the highest value at 20 mA cm^{-2} was observed for phenol and AO7 and the IBU MCE and η_C were only slightly dependent on current density).

4 Conclusions

The Ti/SnO_2–Sb_2O_4 electrode, prepared by alternate Sn and Sb electrodepositions and followed by heating in air at 550 °C to form the respective oxides, was proven to be effective in the degradation of phenol, IBU, AO7, and DIC. The preparation method involves a relatively simple, rapid, and low cost technique. In general the decrease in the various parameters used to follow the degradation was different, as absorbance decreases were larger than for COD or TOC. Interestingly, TOC removals presented, in most cases, the lowest values, which meant that the mechanism of electrodegradation did not move directly to mineralization, but rather followed a pathway that involved the formation of intermediates. This fact was in agreement with the low combustion efficiencies observed that, except for the dye AO7, were found to be dependent on current density. For the remaining experimental conditions tested, ICE was lower than 30% and the relative values of MCE for the different compounds studied followed a trend identical to that of η_C. The electrode was stable throughout the experiments and, if further improvements are made to increase its durability and mineralization efficiency, it can be a good alternative to the expensive BDD anode.

Acknowledgments The financial support of Fundação para a Ciência e a Tecnologia, FCT, BII 2/UMTP/UBI/2008, PTDC/CTM/64856/2006, is gratefully acknowledged.

References

1. Kotz R, Stucki S, Carcer B (1991) J App Electrochem 21:14
2. Vincent CA, Weston DGC (1972) J Electrochem Soc 119:518
3. Aboaf JA, Marcotte VC (1973) J Electrochem Soc 120:701
4. Jarzebski ZM, Marton JP (1976) J Electrochem Soc 123:199C
5. Hsu YS, Ghandhi SK (1979) J Electrochem Soc 126:1434
6. Hsu YS, Ghandhi SK (1980) J Electrochem Soc 127:1592
7. Chen X, Chen G, Yue PL (2001) J Phys Chem B 105:4623
8. Cui YH, Feng YJ, Liu ZQ (2009) Electrochim Acta 54:4903
9. Mahadevaiyer Y, Ramakrishnan KR, Nayak NU et al (1990) J Mater Sci Lett 9:1132
10. Feng Y, Cui Y, Logan B et al (2008) Chemosphere 70:1629
11. Berenguer R, Quijada C, Morallón E (2009) Electrochim Acta 54:5230

12. Chen X, Yao P, Wang D et al (2009) Chem Eng J 147:412
13. Chen X, Gao F, Chen G (2005) J Appl Electrochem 35:185
14. Cossu R, Polcaro AM, Lavagnolo MC et al (1998) Environ Sci Technol 32:3570
15. Stucki S, Kötz R, Carcer B et al (1991) J App Electrochem 21:99
16. Comninellis Ch (1992) Trans IChem E Part B 70:219
17. Rodgers JD, Jedral W, Bunce NJ (1999) Environ Sci Technol 33:1453
18. Johnson DC, Feng J, Houk LL (2000) Electrochim Acta 46:323
19. Szpyrkowicz L, Juzzolino C, Kaul SN et al (2000) Ind Eng Chem Res 39:3241
20. Wang A, Qu J, Liu H et al (2004) Chemosphere 55:1189
21. Li XY, Cui YH, Feng YJ et al (2005) Water Res 39:1972
22. Borras C, Berzoy C, Mostany J et al (2007) Appl Catal B Environ 72:98
23. Mao X, Tian F, Gan F et al (2008) Russ J Electrochem 44:802
24. Cui YH, Li XY, Chen G (2009) Water Res 43:1968
25. Comninellis Ch (1994) Electrochim Acta 39:1857
26. Comninellis Ch, Pulgarin C (1993) J Appl Electrochem 23:108
27. Comninellis Ch, Nerini A (1995) J Appl Electrochem 25:23
28. Pulgarin C, Adler N, Péringer P et al (1994) Water Res 28:887
29. Polcaro AM, Palmas S, Renoldi F et al (1999) J Appl Electrochem 29:147
30. Chen X, Chen G, Gao F et al (2003) Environ Sci Technol 37:5021
31. Yang X, Zou R, Huo F et al (2009) J Hazard Mater 164:367
32. Song S, Zhan L, He Z et al (2010) J Hazard Mater 175:14
33. Hoflung GB, Cox DF (1981) Thin Solid Films 83:261
34. Montilla F, Morallón E, De Battisti A et al (2004) J Phys Chem B 108:5036
35. Montilla F, Morallón E, Vázquez JL (2005) J Electrochem Soc 152:B421
36. Río AI, Molina J, Bonastre J et al (2009) J Hazard Mater 172:187
37. Andrade LS, Rocha-Filho RC, Bocchi N et al (2004) Quim Nova 27:866
38. Correa-Lozano B, Comninellis Ch, De Battisti A (1997) J Appl Electrochem 27:970
39. Chen G, Chen X, Yue PL (2002) J Phys Chem B106:4364
40. Zanta CLPS, Michaud PA, Comninellis Ch et al (2003) J Appl Electrochem 33:1211
41. Adams B, Tian M, Chen A (2009) Electrochim Acta 54:1491
42. Wang Y, Fan C, Hua B et al (2009) Trans Nonferrous Met Soc China 19:78
43. Zhu K, Zhang W, Wang H et al (2008) Clean 36:97
44. Yao P, Chen X, Wu H et al (2008) Surf Coat Technol 202:3850
45. Liu JF, Feng YJ (2009) Sci China Ser E-Tech Sci 52:1799
46. Eaton A, Clesceri L, Greenberg A (2005) Standard methods for examination of water and wastewater, 21st edn. American Public Health Association, Washington
47. Pourbaix M (1963) Atlas D'équilibres Électrochimiques à 25 C. Gauthier-Villars & Cie Éditeur, Paris
48. Levine S, Smith AL (1971) Faraday Discuss Chem Soc 52:290
49. Ciríaco L, Anjo C, Correia J et al (2009) Electrochim Acta 54:1464
50. Iniesta J, Michaud A, Panizza M et al (2001) Electrochem Commun 3:346
51. Boudreau J, Bejan D, Li S et al (2010) Ind Eng Chem Res 49:2537
52. Pacheco MJ, Morão A, Lopes A et al (2007) Electrochim Acta 53:629
53. Comninellis Ch, Pulgarin C (1991) J Appl Electrochem 50:949
54. Brillas E, Sirés I, Arias C et al (2005) Chemosphere 58:399